

# Use of Butylamine Modified Graphene Sheets as Transparent Electrodes in Polymer Solar Cells

Luca Valentini<sup>a\*)</sup>, Marta Cardinali<sup>a)</sup>, Silvia Bittolo Bon <sup>a)</sup>, Diego Bagnis<sup>a)</sup>, Raquel Verdejo<sup>b)</sup>, Miguel A. Lopez-Manchado<sup>b)</sup>, Jose M. Kenny<sup>a),b)</sup>

*a) Dipartimento di Ingegneria Civile e Ambientale, Università di Perugia, INSTM, UdR Perugia, 05100 Terni – Italy.*

*b) Instituto de Ciencia y Tecnología de Polimeros, CSIC, Juan de la Cierva, 3, 28006 Madrid, Spain.*

We describe a facile method to use soluble chemically derived graphene sheets (GSs), which has a one-atom thickness and a two-dimensional structure, as transparent electrode for the preparation of polymer solar cells. Chemically functionalized GSs were obtained by first covalently attaching fluorine and then exposing the obtained fluorinated graphene sheets to an aliphatic amine at room temperature. Scanning electron microscopy, atomic force microscopy and UV-Vis analyses confirmed the obtaining of transparent graphene sheets with an average thickness of 0.7-0.9 nm. A proof-of-concept application in a polymer solar cell is demonstrated. The functionalized graphene, which is cheap and easily prepared, is expected to be a competitive candidate as hole acceptor material in polymer photovoltaic applications.

\* To whom correspondence should be addressed. E-mail: mic@unipg.it.

## Introduction

Graphene, which consists of a two-dimensional (2D) sheet of covalently bonded carbon atoms, has unique electronic property and can be considered as a nanometer-scale building block for new nanomaterials<sup>1</sup> with different device applications, such as field-effect transistors<sup>2</sup>, resonators<sup>3</sup>, transparent anodes<sup>4</sup> and organic photovoltaic devices have been reported.<sup>5</sup> Graphene sheets can be prepared by various techniques including mechanical exfoliation of graphite<sup>2</sup> and reduction of exfoliated graphite oxide.<sup>6</sup> As perfect graphene itself does not exist, the development of methods that allow processing of graphene sheets has become a top priority.

An ideal monolayer of graphene has transparency of 98%<sup>7</sup> with sheet resistance of 6 k $\Omega$ /sq, making it suitable for transparent and conducting electrodes. However, for technological feasibility, uniform deposition over large areas is necessary. The functionalization of graphene has been considered to be important for improving their solubility and self-assembly properties, and applications in devices.<sup>8</sup> So far, chemical functionalization of graphene has focused on improving its solubility/processability in both water and organic solvents using different soluble groups.<sup>9-14</sup>

Soluble chemically converted graphene oxide has been used as acceptor material into the active layer of bulk heterojunction polymeric solar cells.<sup>15-17</sup> In other cases the reduced graphene oxide has been used as transparent anode.<sup>18-20</sup> For the bulk heterojunction solar cells, at our best knowledge, it was not studied the effects of graphene and a hole-trapping conducting polymer on the morphological and electrical properties of the polymeric photoactive layer when they are used as a composite material for the realization of an anode.

More recently, with a novel approach it is demonstrated that the direct fluorination of graphene sheets and their subsequent derivatization provides a versatile tool for the preparation of single graphene sheet.<sup>21-23</sup>

This last method has been used in this paper to fabricate transparent poly(3,4-ethylenedioxythiophene:poly(styrenesulfonate)/graphene composite films by spin coating. The composite film coated indium tin-oxide electrode was used as anode for polymer bulk heterojunction

solar cells reaching an overall power conversion efficiency of 0.75% upon the excitation of 100 mWcm<sup>-2</sup> AM 1.5 white light.

## Results and discussion

Theoretical investigation reveals that monocrystalline graphite belongs to the  $D_{6h}^4$  space-group symmetry. Thus, an out-of-plane  $A_{2u}$  mode around at 868 cm<sup>-1</sup> and an in-plane  $E_{1u}$  mode around at 1588 cm<sup>-1</sup> are infrared-active.<sup>24,25</sup> A typical FTIR spectrum of the F-GSs is shown in Figure 1a. We found the  $A_{2u}$  mode around at 839 cm<sup>-1</sup> and the  $E_{1u}$  mode at 1590 cm<sup>-1</sup>.

The IR spectrum of F-GS also illustrates the peaks at 1060 and 1730 cm<sup>-1</sup> which are characteristics of the C-O and C=O stretches of the graphene sheets.<sup>23</sup> C-F vibration modes are located in the 1000–1400 cm<sup>-1</sup> region, including -CF<sub>2</sub> stretching mode at 1120 cm<sup>-1</sup><sup>26</sup> and F-aryl mode at 1150 and 1260 cm<sup>-1</sup>.<sup>27</sup> The mechanism of interaction between fluorinated graphenes and primary amine proceeds via elimination of fluorine and the formation of N–H bond. IR spectroscopy was used to verify the occurrence of this reaction by dispersing our F-GSs in a commercial primary aliphatic amine such as butylamine at room temperature (Figure 1b). The absorptions of the primary amine at 3290 and 3370 cm<sup>-1</sup>, due to asymmetric and symmetric N-H stretching vibrations<sup>28</sup> of the BAM when it was mixed with the GSs, changed after its reaction with F-GS and formed a broad band at 3400 cm<sup>-1</sup> attribute to a secondary amine. XPS analysis shows how the fluorine atoms have been substituted from the nitrogen atoms after the treatment with the butylamine moiety (Table 1). These findings suggest that the mechanism of interaction between fluorinated graphenes and primary amine proceeds via elimination of fluorine and the formation of N–H bond.

Field emission scanning electron microscopy was used to obtain direct visualization of GSs and F-GSs dispersed in butylamine. In the case of neat GSs, what is observed is an agglomeration of isolated fluffy structures (Figure 2a). It is also clear that after dispersing the F-GSs in butylamine using sonication, the

graphene sheets were dispersed uniformly onto the substrate and they appeared flattened after the amine functionalization (Figure 2b).

Atomic force microscopy, AFM, has been used as direct method of quantifying the degree of exfoliation to graphene sheet level. Tapping mode AFM image and the height profile of the BAM modified F-GSs is reported in Figure 3. Amino functionalized F-GSs was previously diluted in DMF and then cast on a glass support before its observation by AFM. Well-dispersed graphene sheets have been obtained. Graphene sheets with average thickness of 0.7-0.9 nm were observed, which is characteristic of exfoliated graphene sheet.<sup>29,30</sup>

In order to investigate the role played by the graphene exfoliation on the optical transparency, GSs and amine modified F-GSs were deposited on glass substrates and further characterized by UV-Vis spectroscopy at normal incidence. The graphene morphology had the most direct effect on transmittance, as is evident in the spectra presented in Figure 4. As expected, higher degree of exfoliation delivered thinner films that were more optically transparent, with those obtained from BAM modified F-GSs displaying optical transmittances of 97% at 550 nm. Note that for neat graphene a decrease of the overall absorbance has been observed.

Four-point sheet resistance measurements were then made. The PEDOT:PSS/GSs film showed a sheet resistance of 1500 k $\Omega$ /sq. Control experiments were also performed on neat PEDOT:PSS and PEDOT:PSS/BAM modified F-GSs films, which reveal sheet resistances of  $3 \times 10^5$  k $\Omega$ /sq and 800 k $\Omega$ /sq, respectively. To explain the decrease of the sheet resistance of the PEDOT:PSS/BAM modified F-GS electrode, we suggest as reported in Figure 2b the formation of an extended conjugated network with individual graphene bridging the gaps between graphene sheets.

The role played by these graphene modified electrodes on the crystalline and morphological arrangement of the active layer (i. e. P3HT:PCBM film) of the solar cell device has been investigated by wide angle x-ray scattering, WAXS, and AFM measurements.

The presence of intensive (h 0 0) peaks at about 5° and 11° and the absence of (0 1 0) peak measured in the reflection geometry for the ITO/PEDOT:PSS/GSs/RR-P3HT:PCBM, ITO/PEDOT:PSS/BAM modified F-GSs/RR-P3HT:PCBM and ITO/PEDOT:PSS/RR-P3HT:PCBM films confirmed the orientation effect of P3HT molecular alignment caused by the solution-cast, that is, the side chains (*a*-axis) oriented preferably perpendicular to the film surface, whereas the  $\pi$ - $\pi$  stacking of main chains (*b*-axis) oriented preferably parallel to the film surface.<sup>31</sup> In addition, the morphology of the active layer was found dependent upon the presence of chemically derived graphene sheets as shown in Figure 6.

Tapping mode phase AFM images of the P3HT:PCBM layer deposited onto PEDOT:PSS/GSs and PEDOT:PSS/BAM modified F-GSs electrodes are reported in Figure 6. We choose the phase imaging because the phase shift is very sensitive to the local surface property, such as the rigidity, and the phase shift can extract only the information on the change of the surface property.

From the AFM analysis it was found that the P3HT:PCBM layer deposited onto PEDOT:PSS/GSs electrode (Figure 6a) is less planar (RMS surface roughness 2.6 nm) than those spin-cast onto the PEDOT:PSS/ BAM modified F-GSs one (RMS surface roughness 0.95 nm) (Figure 6b). Moreover, we can see how the appearance of large regions with higher stiffness (i. e. brighter regions) in Figure 6a have been reduced in size with the phase separation that is now taking place in a much smaller scale (Figure 6b).

As reported below, the effect of the chemically functionalized graphene sheets on morphology was found to play a very important role in controlling the heterojunction device performance in particular by increasing the short-circuit current density.

Figure 7 shows the results obtained comparing the performance of the prepared organic solar cells; the average current density–voltage curves of multiple measurements on different electrodes realized on each device (see Supplementary data) are reported in figure 7; the calculated electrical parameters are summarized in Table 2.

Without thermal annealing, the power conversion efficiency for the ITO/PEDOT:PSS/RR-P3HT:PCBM/LiF/Al device is very poor and is almost the same as that measured recently elsewhere.<sup>32</sup>

The short circuit current density ( $J_{SC}$ ), open circuit voltage ( $V_{OC}$ ), fill factor (FF), and power conversion efficiency ( $\eta$ ) are 3.26 mA/cm<sup>2</sup>, 556 mV, 0.41, and 0.75%, respectively, for the active layer on BAM modified F-GSs, and 2.52 mA/cm<sup>2</sup>, 525 mV, 0.29, and 0.38%, respectively, for the cell on neat GSs.

It was demonstrated how in the carbon nanotube-PEDOT composites, the current-voltage data and photoluminescence suggested an electronic interaction between nanotubes and PEDOT; the electronic interaction originates from the hole trapping nature of the carbon nanotubes in a hole-conducting polymer.<sup>33</sup>

More recently it has been demonstrated<sup>18</sup> how similar devices fabricated on neat graphene have an efficiency of approximately 0.1% while devices fabricated with PEDOT:PSS alone were not able to work. Since the electronic properties of graphene are similar to that of nanotubes, the obtained results suggested also that the GSs may interact as hole trapping in hole-conducting polymers. Moreover, as demonstrated by Sariciftci<sup>34</sup> and coworkers the morphology of the active layer plays an outstanding role in the performance of the bulk heterojunction solar cells; in particular it was shown how a smoother morphology with a reduced phase separation improves the performance of devices. In fact for efficient devices, the created charge need to be transported to the electrodes within their lifetime. In particular the fill factor is determined by charge carriers reaching the electrodes when the built-in field is lowered toward the open circuit voltage. This means that the use of butylamine modified graphene sheets as anode enhances the charge carrier transport reducing the recombination effect of the active layer.

## **Experimental**

Graphene sheets were produced starting from natural graphite powder (universal grade, 200 mesh, 99.9995%) as previously reported.<sup>21,23</sup> Briefly, graphite powder was dispersed in 20 mL of fuming nitric

acid for 20 min; next, potassium chlorate (8 g) was slowly added over 1 h and the reaction mixture was stirred for 21 h at 0°C. The obtained graphite oxide was thermally exfoliated at 300°C for 3 min under air atmosphere giving rise to graphene sheets (GSs).

The obtained GSs were then ultrasonicated in toluene (2mg/20mL) for 1 h. GS dispersion was spin-cast (1000 rpm) onto indium tin-oxide (ITO)-coated glass (electrical sheet resistivity of 14 Ohm/sq). The material was then annealed at 70°C for 2 h in order to desorb any residual solvent.

Fluorinated graphene sheets (F-GSs) were obtained by the plasma assisted decomposition of CF<sub>4</sub> employing a 13.56 MHz radiofrequency plasma source. The plasma treatment was carried out at room temperature with the CF<sub>4</sub> gas pressure fixed at 10<sup>-2</sup> Torr for 45 min. The CF<sub>4</sub> flow rate was kept constant at 21 sccm. The graphene fluorination was performed with a RF bias voltage fixed at -250 V. A commercially available grade of butylamine (CH<sub>3</sub>(CH<sub>2</sub>)<sub>3</sub>NH<sub>2</sub>, BAM) supplied by Sigma–Aldrich Chemicals, was used in this research. F-GSs were dispersed in the liquid amine using an ultrasonication probe for 1 h in a thermostatic bath at 5°C to avoid the evaporation of the amine.

The morphologies of GSs and amino modified F-GSs were investigated by field-emission scanning electron microscopy and atomic force microscopy (AFM) Nanoscope IV from Digital Instruments. AFM images were obtained in tapping mode. Infrared (IR) (KBr pellets method) and X-ray photoelectron spectroscopes were used to confirm the presence of covalently bound fluorine and the amino functionalization of the F-GSs.

The poly(3,4-ethylenedioxythiophene (PEDOT):poly(styrenesulfonate) (PSS) (purchased from Aldrich, PEDOT and PSS content 0.5 wt.% and 0.8 wt.% respectively, 1.3 wt.% dispersion in H<sub>2</sub>O) was spin-cast (4000 rpm for 1 min) onto the ITO substrate, and was subsequently dried at 150°C for 1 hr in air. The thickness of the PEDOT:PSS layer was 50 nm.

The GSs and amine modified F-GSs were spin-cast (1000 rpm) onto the PEDOT:PSS coated ITO substrate. The sheet resistance of PEDOT:PSS and PEDOT:PSS/graphene films was obtained by four point probe measurements. Transmittance of these films was measured by UV-Vis spectrometer.

Regioregular poly(3-hexylthiophene) (RR-P3HT purchased from Aldrich, molecular weight 46000, used as received) and [6,6]-phenyl C<sub>61</sub>-butyric acid methyl ester (PCBM, purchased from Solenne, used as received) were used for this research.

The solar cells were fabricated with the structures of ITO/PEDOT:PSS/BAM modified F-GSs/RR-P3HT:PCBM/LiF/Al and ITO/PEDOT:PSS/GSs/RR-P3HT:PCBM/LiF/Al, respectively. As reference, a solar cell with the structure of ITO/PEDOT:PSS/RR-P3HT:PCBM/LiF/Al was also fabricated.

The photosensitive layer was prepared spin coating (1000 rpm, 20s) from an *o*-dichlorobenzene (ODCB) solution of the RR-P3HT:PCBM (1:1 weight ratio) blend with the solution concentration of 20 mg\*ml<sup>-1</sup> onto the ITO/PEDOT:PSS/graphene electrode. The thickness of spin-cast photosensitive layer was 100 nm as estimated by AFM. The thickness of the layers has been determined by depositing each layer and removing it with an appropriate solvent. Then the top metal electrode, which is made up of LiF and Al, was deposited on the active layer by vacuum evaporation ( $\approx 10^{-6}$  Torr) with an optimized thickness of 0.7 and 60 nm, respectively, through a shadow mask consisting of stripes with 2 mm width and 2 mm length. The device layout consists of PEDOT:PSS, graphene and the photoactive layer sandwiched between patterned and crossed ITO and LiF/Al stripes as electrodes. The area of each device is the crossing portions of the patterned electrodes.

The current-voltage (I-V) measurement of the devices was conducted on a computer-controlled Keithley 4200 Source Measure Unit. The photocurrent was measured under AM1.5D 100 mWcm<sup>-2</sup> (P<sub>in</sub>) illumination from a Thermal Oriel solar simulator. The performance of each cell was measured positioning the photovoltaic device on the maximum optical power measured at the sample with a radiant power energy meter Newport 70260.

The AFM and Wide-Angle X-ray Scattering (WAXS) experiments were carried out on the spin-cast films of ITO/PEDOT:PSS/RR-P3HT:PCBM, ITO/PEDOT:PSS/BAM modified F-GSs/RR-P3HT:PCBM and ITO/PEDOT:PSS/RR-P3HT:PCBM. The WAXS experiment was done by using an ATX-G diffractometer in reflection mode with a parallel beam optics attachment. The instrument was

operated at a 50 kV voltage and a 240 mA current and was calibrated with a standard silicon sample. Copper K $\alpha$  radiation ( $\lambda=0.154$  nm) was used.

## **Conclusion**

We have developed a novel approach able to lead to a stable dispersion of individual graphene sheets when they were exposed to organic moieties. We demonstrated that such soluble graphene sheets can be used as transparent conductive electrodes for polymer photovoltaic cells. Besides the one-atom-thick plane structure feature, large specific area, and the inertness against oxygen and water vapor of graphene make this material a promising candidate in photovoltaic applications.

## **Acknowledgments**

The authors of this study gratefully acknowledge the financial support of the Ministry of Science and Education (MEC, Spain) through its project MAT 2007-61116.

## References

- 1 A. K. Geim, K. S. Novoselov, *Nature Mater.*, **2007**, *6*, 183.
- 2 K. S. Novoselov, A. K. Geim, S. V. Morozov, D. Jiang, Y. Zhang, S. V. Dubonos, I. V. Grigorieva, A. A. Firsov, *Science*, **2004**, *306*, 666.
- 3 J. S. Bunch, A. M. van der Zande, S. S. Verbridge, I. W. Frank, D. M. Tanenbaum, J. M. Parpia, H. G. Craighead, P. L. McEuen, P. L. *Science*, **2007**, *315*, 490.
- 4 H. A. Becerril, J. Mao, Z. F. Liu, R. M. Stoltenberg, Z. N. Bao, Y. S. Chen, *ACS Nano*, **2008**, *2*, 463.
- 5 Z. F. Liu, Q. Liu, X. Y. Zhang, Y. Huang, Y. F. Ma, S. G. Yin, Y. S. Chen, *Adv. Mater.*, **2008**, *20*, 3924.
- 6 D. Li, R. B. Kaner, *Science*, **2008**, *320*, 1170.
- 7 R. R. Nair, P. Blake, A. N. Grigorenko, K. Novoselov, T. J. Booth, T. Stauber, N. M. R. Peres, A. K. Geim, *Science*, **2009**, *323*, 610.
- 8 Y. C. Si, E. T. Samulski, *Nano Lett.*, **2008**, *8*, 1679.
- 9 S. Niyogi, E. Bekyarova, M. E. Itkis, J. L. McWilliams, M. A. Hamon, R. C. Haddon, *J. Am. Chem. Soc.* **2006**, *128*, 7720.
- 10 Y. X. Xu, H. Bai, G. W. Lu, C. Li, G. Q. Shi, *J. Am. Chem. Soc.*, **2008**, *130*, 5856.
- 11 S. Stankovich, D. A. Dikin, G. H. B. Dommett, K. M. Kohlhaas, E. J. Zimney, E. A. Stach, R. D. Piner, S. T. Nguyen, R. S. Ruoff, *Nature*, **2006**, *442*, 282.
- 12 S. Stankovich, R. D. Piner, S. T. Nguyen, R. S. Ruoff, *Carbon*, **2006**, *44*, 3342.
- 13 Y. C. Si, E. T. Samulski, *Nano Lett.*, **2008**, *8*, 1679.
- 14 G. Eda, G. Fanchini, M. Chhowalla, *Nat. Nanotechnol.*, **2008**, *3*, 270.
- 15 L. Qian, L. Zunfeng, Z. Xiaoyan, Y. Liying, Z. Nan, P. Guiling, Y. Shougen, C. Yongsheng, W. Jun, *Adv. Funct. Mater.* **2009**, *19*, 894.
- 16 L. Zunfeng, L. Qian, H. Yi, M. Yanfeng, Y. Shougen, Z. Xiaoyan, S. Wei, C. Yongsheng, *Adv. Mater.* **2008**, *20*, 3924.

- 17 Q. Liu, Z. Liu, X. Zhang, N. Zhang, L. Yang, S. Yin, Y. Chen. *Appl. Phys. Lett.*, **2008**, 92, 223303.
- 18 G. Eda, Y. Y. Lin, S. Miller, C. W. Chen, W. F. Su, M. Chhowalla, *Appl. Phys. Lett.*, **2008**, 92, 233305.
- 19 V. C. T, Li-Min Chen, M. J. Allen, J. K. Wassei, K. Nelson, R. B. Kaner, Y. Yang. *Nano Lett.*, **2009**, 9 (5), 1949.
- 20 J. Wu, H. A. Becerril, Z. Bao, Z. Liu, Y. Chen, P. Peumans, *Appl. Phys. Lett.*, **2008**, 92, 263302.
- 21 R. Verdejo, F. Barroso-Bujans, M. A. Rodriguez-Perez, J. A. de Saja, M. A. Lopez-Manchado, *J. Mater. Chem.*, **2008**, 18, 2221.
- 22 S. Bittolo Bon, L. Valentini, R. Verdejo, J. L. Garcia Fierro, L. Peponi, M. A. Lopez-Manchado, J. M. Kenny, *Chem. Mater.*, **2009**, 21, 3433.
- 23 Y. Liang, D. Wu, X. Feng, K. Mullen, K. *Adv. Mater.*, **2009**, 21, 1.
- 24 D. S. Knight, W. B. White, *J. Mater. Res.*, **1989**, 4, 385.
- 25 J. Kastner, T. Pichler, H. Kuzmany, S. Curran, W. Blau, D. N. Weldon, M. Delamesiere, S. Draper, H. Zandbergen, *Chem. Phys. Lett.*, **1994**, 221, 53.
- 26 B. N. Khare, P. Wilhite, M. Meyyappan, *Nanotechnology*, **2004**, 15, 1650.
- 27 A. Felten, C. Bittencourt, J. J. Pireaux, *J. Appl. Phys.*, **2005**, 98, 093123.
- 28 D. H. Williams, I. Fleming, In *Spectroscopic Methods in Organic Chemistry*, McGraw-Hill Companies, 1969.
- 29 S. Niyogi, E. Bekyarova, M. E. Itkis, J. L. McWilliams, M. A. Hamon, R. C. Haddon, *J. Am. Chem. Soc.*, **2006**, 128, 7720.
- 30 Y. X. Xu, H. Bai, G. W. Lu, C. Li, G. Q. Shi, *J. Am. Chem. Soc.* **2008**, 130, 5856.
- 31 K. E. Aasmundtveit, E. J. Samuelsen, M. Guldstein, C. Steinsland, O. Flornes, C. Fagermo, T. M. Seeberg, L. A. A. Pettersson, O. Inganas, R. Feidenhans, S. Ferrer, *Macromolecules*, **2000**, 33, 3120.
- 32 Honda S, Nogami T, Ohkita H, Benten H, Ito S. Improvement of the light-harvesting efficiency in polymer/fullerene bulk heterojunction solar cells by interfacial dye modification. *Appl. Mater. Interfaces* 2009; 1:804.

- 33 H. S. Woo, R. Czerw, R.; S. Webster, D. L. Carroll, J. W. Park, J. H. Lee, J. H., *Synth. Met.*, **2001**, 116, 369.
- 34 C. J. Brabec, N. S. Sariciftci, J. C. Hummelen Hummelen, *Adv. Funct. Mater.*, **2001**, 11, 15.

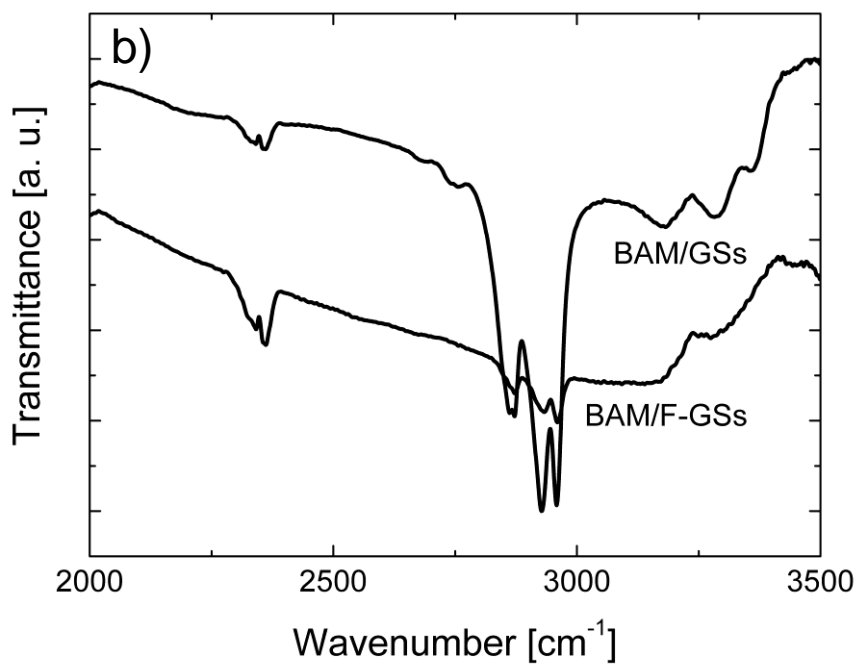
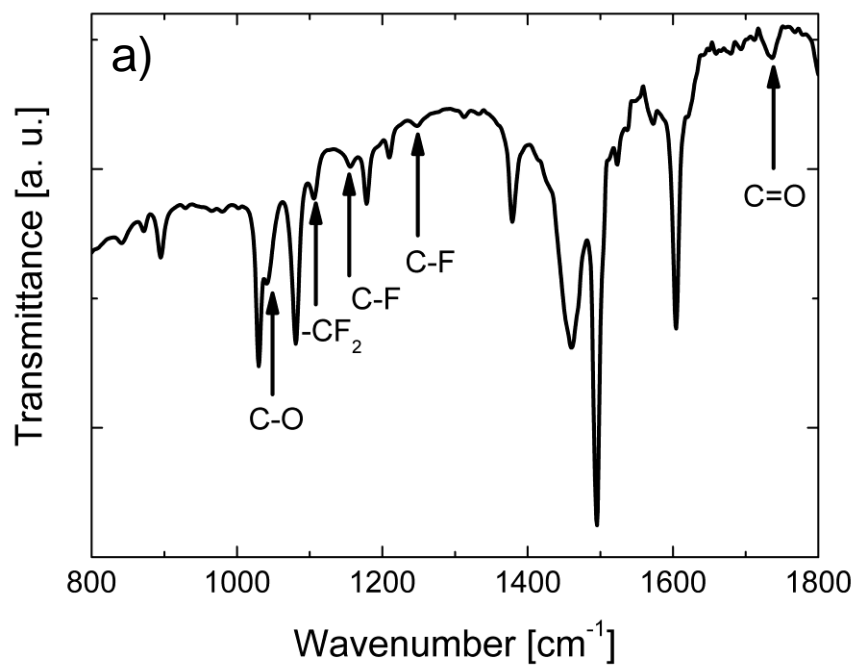


Figure 1: IR spectra of (a) F-GSs and (b) GSs and F-GS derivatives produced by reactions with butylamine (BAM/GSs and BAM/F-GSs, respectively).

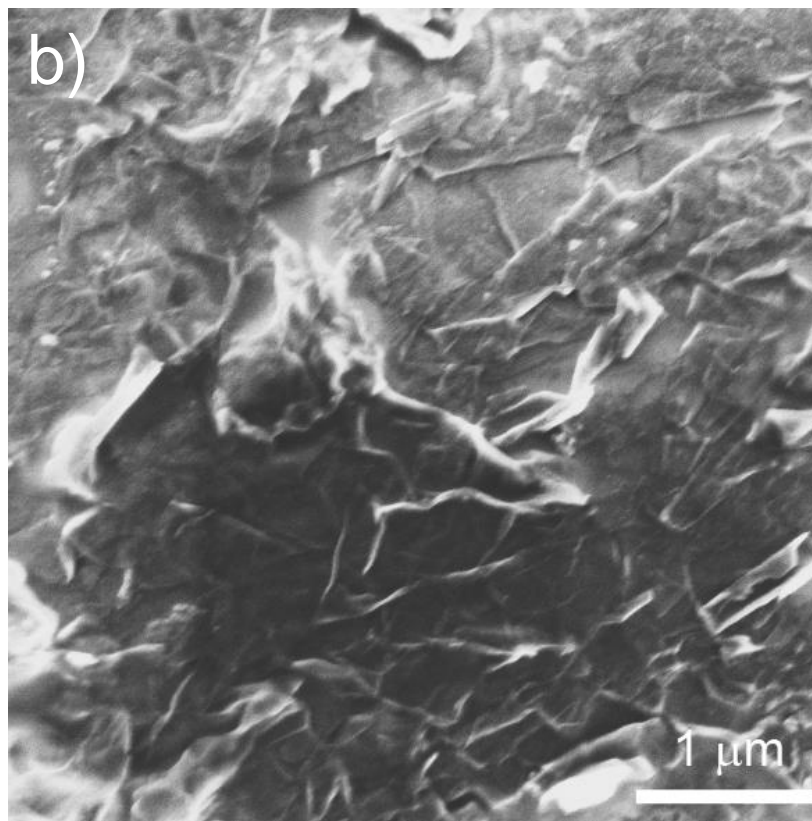
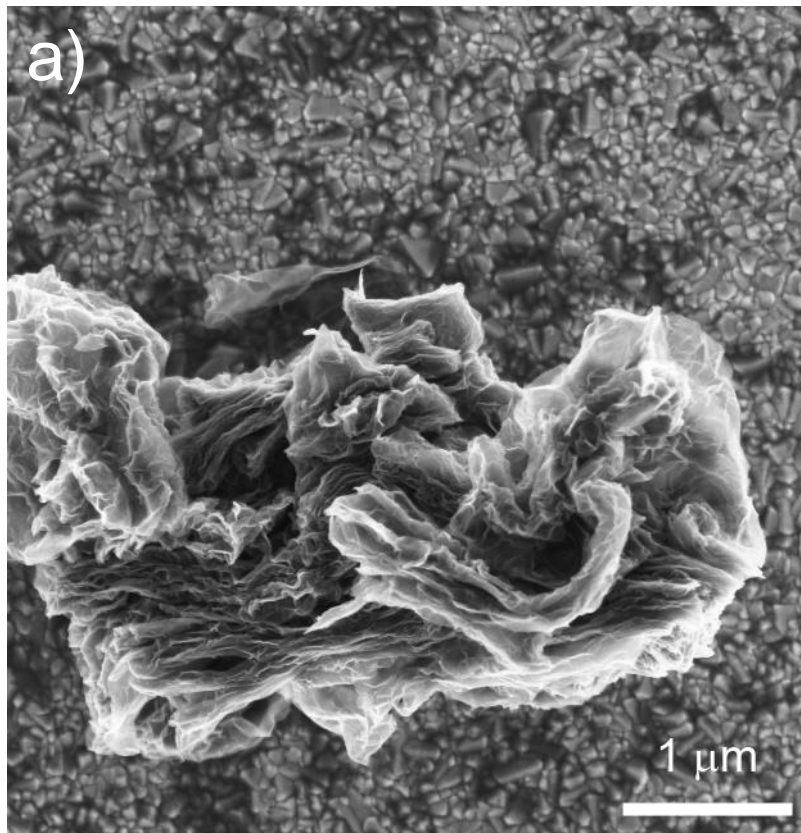


Figure 2: FE-SEM images for (a) neat GSs and (b) BAM modified F-GSs.

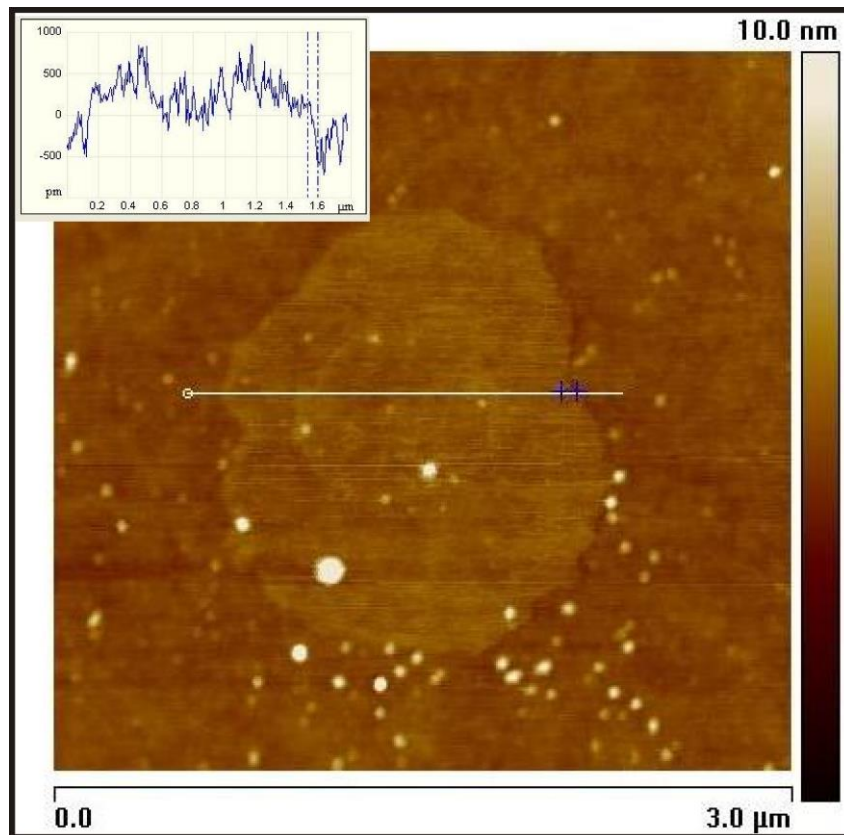


Figure 3: 2D tapping-mode topography ( $2 \mu\text{m} \times 2 \mu\text{m}$ ) AFM image and the height profile of BAM modified F-GSs.

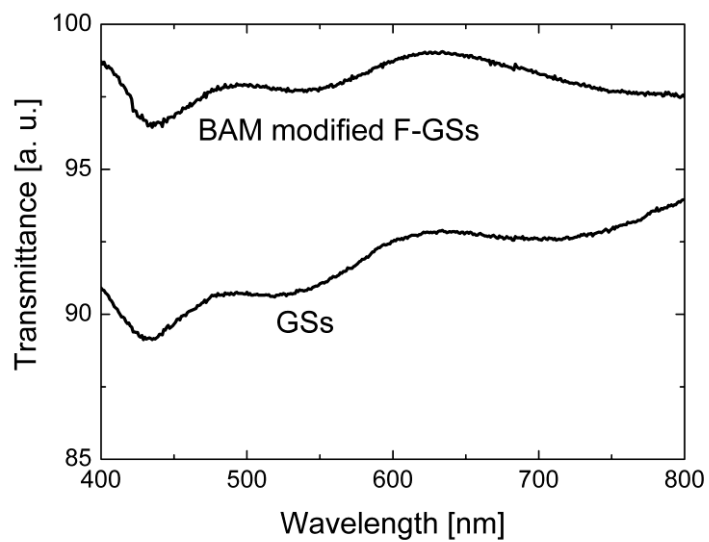


Figure 4: Optical transmittance of GSs and BAM modified F-GSs.

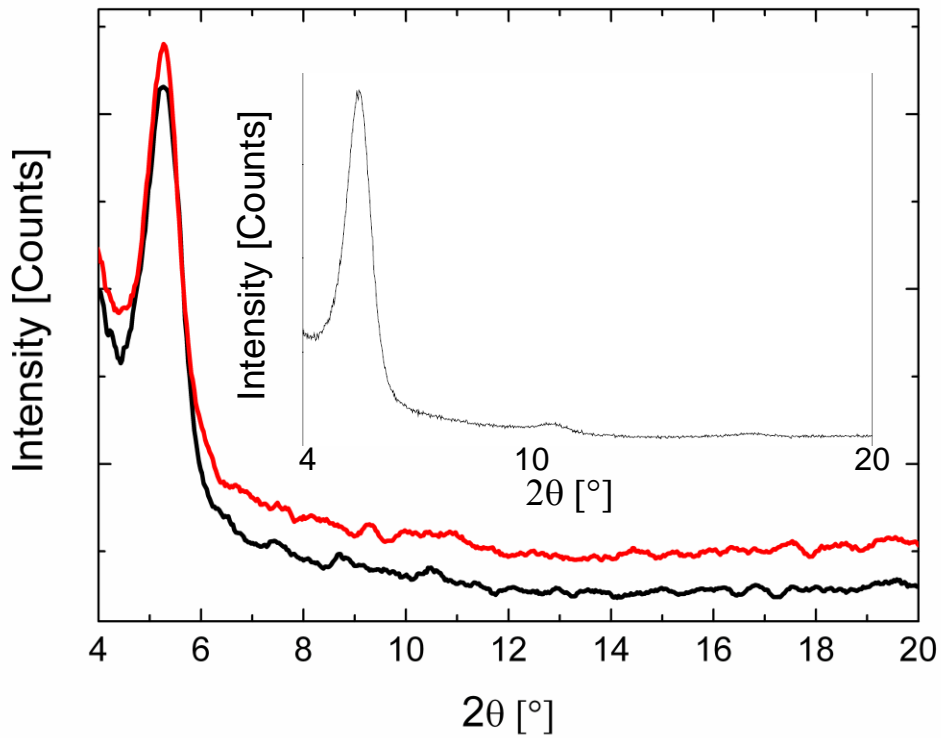


Figure 5: X-ray diffraction patterns in reflection geometry of ITO/PEDOT:PSS/GSs/RR-P3HT:PCBM (red), ITO/PEDOT:PSS/BAM modified F-GSs/RR-P3HT:PCBM (black) films. The inset shows the X-ray diffraction pattern of ITO/PEDOT:PSS/RR-P3HT:PCBM film.

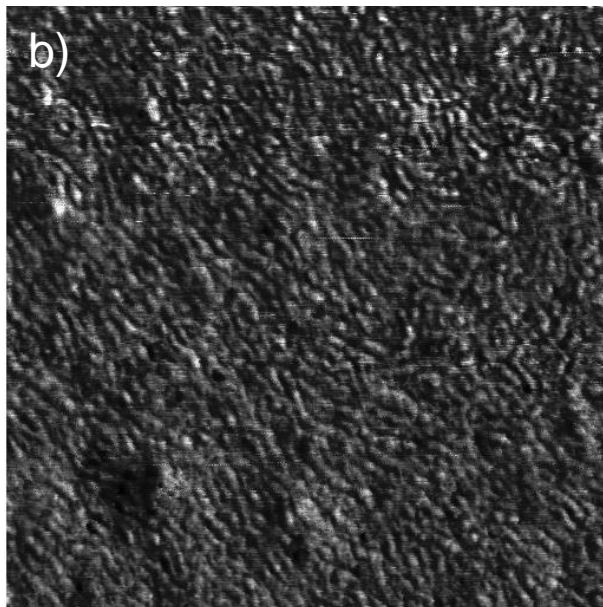
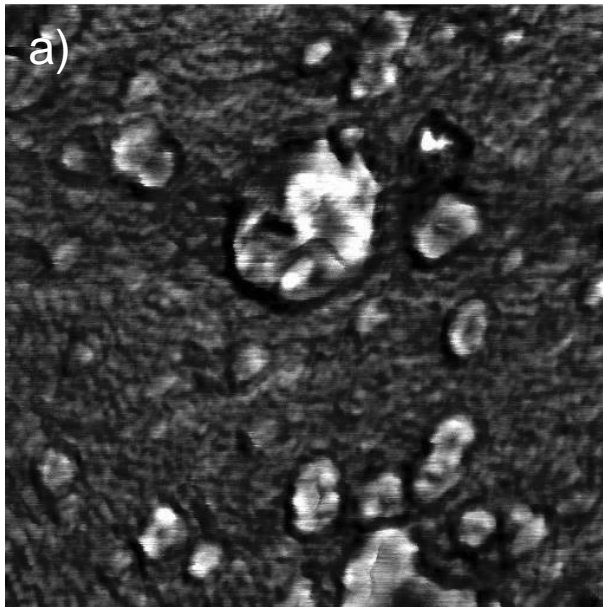


Figure 6: 2D tapping-mode AFM phase images ( $1\ \mu\text{m} \times 1\ \mu\text{m}$ ) of (a) ITO/PEDOT: PSS/GSs/RR-P3HT:PCBM and (b) ITO/PEDOT:PSS/BAM modified F-GSs RR-P3HT:PCBM films.

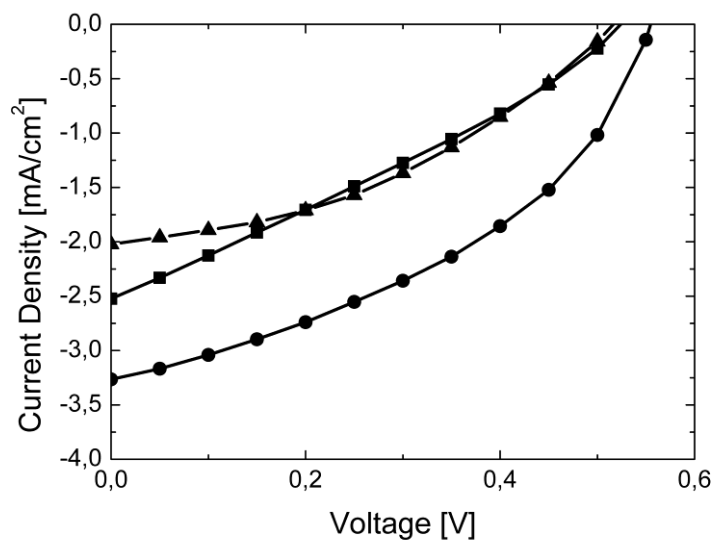


Figure 7: Average current density-voltage curves (under illumination) of the polymer solar cells fabricated by using as anode ITO/PEDOT:PSS (▲), ITO/PEDOT:PSS/GSs (■) and ITO/PEDOT:PSS/BAM modified F-GSs (●) films.

Table 1: Atomic percentage for the analyzed samples.

Table 1.<sup>22</sup>

Samples	At/C
GSs	C/O 1/0.15
F-GSs	C/O/F 1/0.11/1.12
BAM modified F-GSs	C/O/N 1/0.10/0.06

Table 2: Solar cell characteristics: open-circuit voltage ( $V_{oc}$ ), short-circuit current density ( $J_{sc}$ ), fill factor (FF) and power conversion efficiency ( $\eta$ ) for the prepared films. The power conversion efficiency of the photovoltaic cells was calculated using the following equations:  $\eta = FF * V_{oc} * J_{sc} / P_{in}$ .

<b>Device</b>	<b><math>V_{oc}</math></b> <b>[mV]</b>	<b><math>J_{sc}</math></b> <b>[mA/cm<sup>2</sup>]</b>	<b>FF</b>	<b><math>\eta</math></b> <b>[%]</b>
<b>ITO/PEDOT:PSS/GSs/RR-P3HT:PCBM/LiF/Al</b>	525	2.52	0.29	0.38
<b>ITO/PEDOT:PSS/BAM modified F-GSs/RR-P3HT:PCBM/LiF/Al</b>	556	3.26	0.41	0.75
<b>ITO/PEDOT:PSS/RR-P3HT:PCBM/LiF/Al</b>	514	2.02	0.41	0.41